# Supporting Information for "Gravitational constraints on the Earth's inner core differential rotation"

Hugo Lecomte[1], Séverine Rosat[1], Mioara Mandea[2], Mathieu Dumberry[3]

[1]Université de Strasbourg, CNRS, EOST, ITES UMR7063, F-67000 Strasbourg, France

[2]Centre National d'Etudes Spatiales, Paris, France

[3]Department of Physics, University of Alberta, Edmonton, Canada

## Contents of this file



## Introduction

The Supporting Information contains the details about the $\alpha$ constraint based on LOD variation (Text S1, Figure S1, and S2), a table that summarize $\delta h$ values estimates (Table S1), details on the $\alpha$ constraint based on GRACE $S_{2,2}$ time-series (Text S3, Figure S3, and Table S2) and details on the $\alpha$ constraint from $C_{2,2}$ time series (Text S4, Figure S4 and Table S3).

## S1. Length of Day (LOD) time-series

We use the IERS EOP C01 (1846-2023) and C04 (1976-2023) LOD time-series (Bizouard, 2020) corrected for zonal tides and for atmospheric, oceanic, hydrologic and sea level angular momentum obtained from the operational products of the Earth-System-Modelling group at GFZ (Dobslaw & Dill, 2018). Note that apart from atmospheric angular momentum the correction from the other sources does not significantly change the time-series at interannual and decadal periods (Rekier et al., 2022; Rosat & Gillet, 2023).

Figure S1 shows the C01 and C04 LOD time-series, band-pass filtered such that the amplitude of the signal is preserved (though note that edge effects reduce the amplitude of the oscillation), and for two different ranges of periods. Over the past 70 years, the amplitude of the LOD changes is approximately 1 ms for decadal (30-yr period) changes, and 0.2 ms for the 6 year period. The longer C01 time-series allows us to see more variations through time and, therefore, the amplitude of the signals is greater than that of C04. The largest peak-to-peak change occurs in the 1960s and 1970s. Figure S2 shows the values of $\alpha$ for each time-series for the range of $\Gamma \in [3 \times 10^{19} - 2 \times 10^{20}]$ N m (Davies et al., 2014) based on Equation 9.

**S2.** $\delta h$ **values estimated in different studies.**

## S3. GRACE solutions of $S_{2,2}$

To verify the IGG-SLR product, it has been compared with GRACE products from three analysis centers. We have selected time-series from ITSG-Grace2018 + ITSG-Grace_operational provided by Graz University of Technology (referred as GRAZ) (Mayer-Gürr et al., 2018), GRACE(-FO) Level-2 (Release-06.1) provided by Center for Space Research (CSR) and referred as CSR (*CSR RL6.0*, 2018) and the International Combination Service for Time-variable Gravity Fields product : COST-G (Grace-RL01 and Grace-FO-RL02) (Meyer et al., 2020). These three time-series span from April 2002 to December 2022. Each solution was prepared with a sub-monthly atmospheric and oceanic loading de-aliasing (Dobslaw et al., 2017) and only GRAZ products uses sub-monthly hydrology de-aliasing. To access interannual timescales, we have applied a low-pass filter with a cut-off period of 3 years, and used a Hamming window to reduce the apodization effect.

As for the LOD variations, interannual variations in $S_{2,2}$ GRACE products are caused by different processes. These include atmospheric and oceanic loadings which are normally corrected by the AOD1B RL06 product (Dobslaw et al., 2017). However, the time-series still contain uncorrected signals from the atmosphere and the ocean, but negligible compared to other processes. The post-glacial rebound, cryospheric loading and sea level rise influence the long-term trend, but their interannual variability is negligible, particularly when we consider $S_{2,2}$ pattern localized on the equator. Hydrological loading and Earth's interior mass redistribution are not corrected in the gravity data.

The three $S_{2,2}$ products from GRACE are very similar in the temporal and spectral domains with only small amplitude variations (Fig. S3a). The IGG-SLR time-series and GRACE $S_{2,2}$ time-series match well after 2010, but differ notably near 2007. The oscillation around that time is also present in the ISBA model, but is not captured in the IGG-SLR time-series. IGG-SLR contains more spectral energy than GRACE products (Fig. S3b). This is explained by the large oscillation in the IGG-SLR product between 1998 and 2002 that is also present in the ISBA model and therefore corresponds to a hydrological signal.

Upper bounds of $\alpha$ from GRACE time-series can be given with a supposed value of $\delta h = 90$ m and for periods of 4 and 6-10 years (Table S2). These constraints are smaller than those based on IGG-SLR because of the differences in spectral content and data length.

## S4. Constraint from $C_{2,2}$

Figure S4a shows the time-series of $C_{2,2}$ from the IGG-SLR product, the ISBA model, and what we refer to henceforth as the corrected $C_{2,2}$ signal (ISBA subtracted from IGG-SLR). Their associated periodograms are shown in Figure S4b. To access inter-annual time scales, we have applied a low-pass filter with a cut-off period of 3 years, and used a Hamming window to reduce the apodization effect. The IGG-SLR time-series contains large signals at periods of 6.5 and 9.5 years. After the correction with the ISBA model, the spectral content of the corrected time-series is shifted with one peak at 6 years and one at 8 years.

The periodogram of the corrected $C_{2,2}$ time-series (Fig. S4b) allows us to place upper bounds for two ranges of periods: the peak at 6-6.5 years and the peak between 8 to 10 year. For an assumed $\delta h = 90$ m, approximately the mid-point of the range 49-126 (Davies et al., 2014), the corresponding upper bounds on $\alpha$ are 6°, 8°, respectively.

These two constraints do not restrict the parameter space more than those obtained with $S_{2,2}$ because of the $\alpha^2$ dependence in equation 7b. This also reflects the fact that the corrected $C_{2,2}$ time-series still contains signals related to surface processes (hydrological, atmosphere or oceanic loadings) even after correction from an hydrological loading model.

## References

Bizouard, C. (2020). *Geophysical Modelling of the Polar Motion.* Walter de Gruyter GmbH & Co KG.

*CSR RL6.0.* (2018). Retrieved from `https://podaac.jpl.nasa.gov/dataset/GRACE_GSM_L2_GRAV_CSR_RL06`

Davies, C. J., Stegman, D. R., & Dumberry, M. (2014). The strength of gravitational core-mantle coupling. *Geophysical Research Letters*, *41*(11), 3786–3792. doi: 10.1002/2014GL059836

Defraigne, P., Dehant, V., & Wahr, J. M. (1996). Internal loading of an inhomogeneous compressible Earth with phase boundaries. *Geophys. J. Int.*, *125*, 173–192.

Dobslaw, H., Bergmann-Wolf, I., Dill, R., Poropat, L., Thomas, M., Dahle, C., ... Flechtner, F. (2017). A new high-resolution model of non-tidal atmosphere and ocean mass variability for de-aliasing of satellite gravity observations: AOD1B RL06. *Geophysical Journal International*, *211*(1), 263–269. doi: 10.1093/gji/ggx302

Dobslaw, H., & Dill, R. (2018). Predicting Earth Orientation Changes from Global Forecasts of Atmosphere-Hydrosphere Dynamics. *Advances in Space Research*, *61*(4), 1047–1054. doi: 10.1016/j.asr.2017.11.044

Mayer-Gürr, T., Behzadpur, S., Ellmer, M., Kvas, A., Klinger, B., Strasser, S., & Zehentner, N. (2018). *ITSG-Grace2018 - Monthly, Daily and Static Gravity Field Solutions from GRACE.* GFZ Data Services.

Meyer, U., Jaeggi, A., Dahle, C., Flechtner, F., Kvas, A., Behzadpour, S., ... Bourgogne, S. (2020). *International Combination Service for Time-variable Gravity Fields (COST-G) Monthly GRACE Series.* GFZ Data Services. doi: 10.5880/ICGEM

.COST-G.001

Rekier, J., Chao, B. F., Chen, J., Dehant, V., Rosat, S., & Zhu, P. (2022). Earth's Rotation: Observations and Relation to Deep Interior. *Surv. Geophys.*, *43*(1), 149–175. doi: 10.1007/s10712-021-09669-x

Rosat, S., & Gillet, N. (2023). Intradecadal variations in length of day: coherence with models of the Earth's core dynamics. *Physics of the Earth and Planetary Interiors*, *submitted*.

Shih, S. A., & Chao, B. F. (2021). Inner core and its libration under gravitational equilibrium: Implications to lower-mantle density anomaly. *Journal of Geophysical Research: Solid Earth*, *126*. doi: https://doi.org/10.1029/2020JB020541

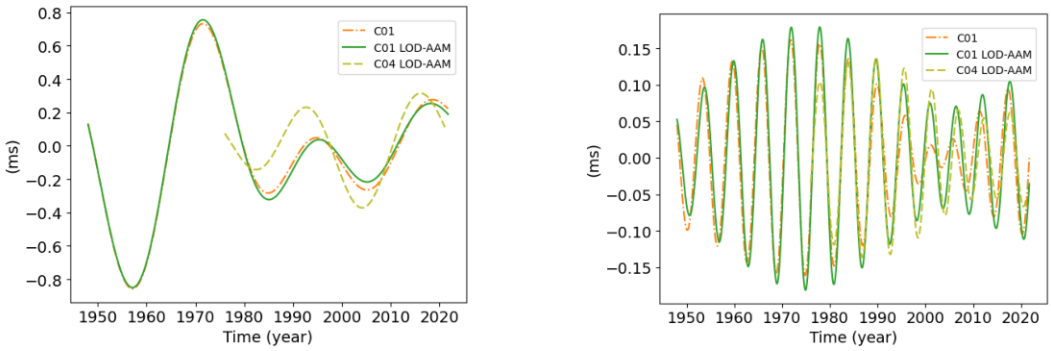


(a) (b)

**Figure S1.** IERS EOP C01 LOD time-series with (green) and without (orange) removal of the Atmopheric Angular Momentum (AAM) contribution and C04 LOD time-series - AAM (lime green). The band-pass filters are (a) between 21 and 50 years, and (b) between 5.5 and 6.5 years.

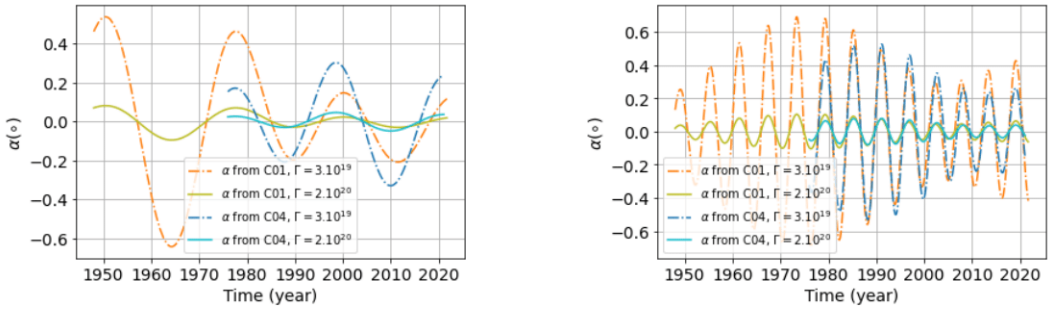


(a) (b)

**Figure S2.** $\alpha$ estimated from the IERS EOP C01 LOD - AAM time-series (orange and lime) and the C04 LOD - AAM time-series (blue and light blue) for the range values of $\Gamma \in [3 \times 10^{19} - 2 \times 10^{20}]$ N m. The band-pass filters are (a) between 21 and 50 years, and (b) between 5.5 and 6.5 years.

| method | $\delta h$ (m) | Reference |
|---|---|---|
| MF | 70 | (Defraigne et al., 1996) |
| MF | 49-126 | (Davies et al., 2014) |
| MICG(2) | 154 | (Davies et al., 2014) |
| MICG(1-2) | 76-164 | (Shih & Chao, 2021) |

**Table S1.** MF = mantle flow models, MICG(x) = mantle inner core gravitational mode period equal to 6 yr, involving the inner core alone (x=1) or the whole of the tangent cylinder (x=2). Note that the numerical values of $\delta h$ were not given explicitly in Davies et al. (2014), but are computed based on their Eq. 3.

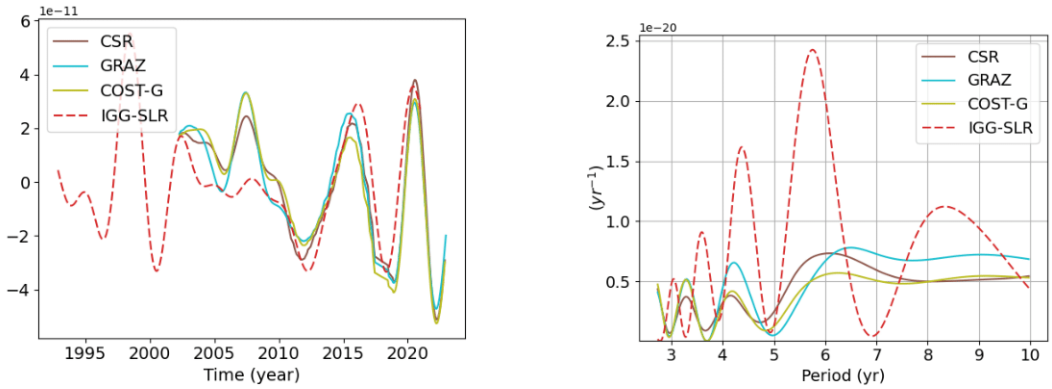


(a) (b)

**Figure S3.** Time-series (a) and Lomb-Scargle periodogram (b) of $S_{2,2}$ coefficient for GRACE CSR (brown), GRAZ (light blue) and COSTG (lime) products and for IGG-SLR (red) product

| | Observation Period (years) | |
|---|---|---|
| | 4 | 6-10 |
| CSR | $0.3^o$ | $0.5^o$ |
| GRAZ | $0.4^o$ | $0.5^o$ |
| COST-G | $0.3^o$ | $0.4^o$ |

**Table S2.** Upper bound values of $\alpha$ based on the GRACE $S_{2,2}$ time-series for different periods considering $\delta h = 90m$.

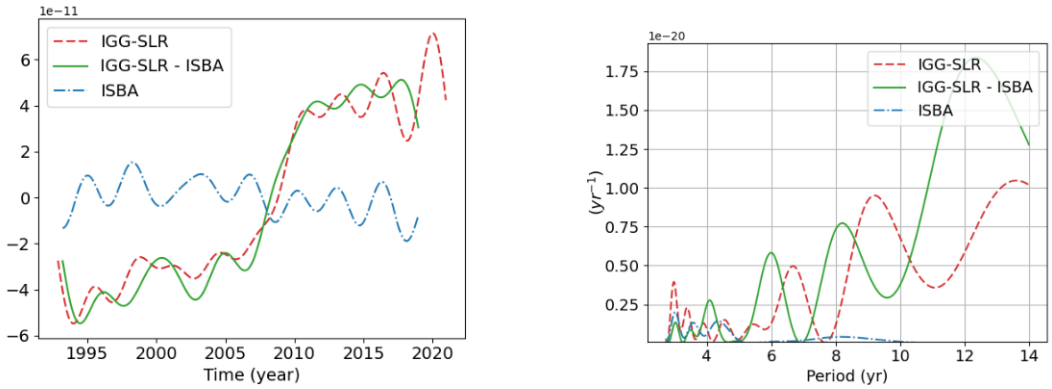


**Figure S4.** Time-series (a) and Lomb-Scargle periodogram (b) of $C_{2,2}$ coefficient for IGG-SLR (red) product, IGG-SLR minus ISBA combination (green) and ISBA (blue)

| Observation | Period (years) | |
|---|---|---|
| | 6-7 | 8-12 |
| IGG-SLR | $5^o$ | $11^o$ |
| IGG-SLR - ISBA | $6^o$ | $8^o$ |

**Table S3.** Upper bound values of $\alpha$ based on the $C_{2,2}$ time-series and for $\delta h = 90$ m.